

PAPER

## Strain-tuning of the magnetocaloric transition temperature in model FeRh films

To cite this article: M G Loving *et al* 2018 *J. Phys. D: Appl. Phys.* **51** 024003

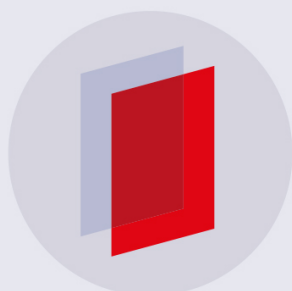
View the [article online](#) for updates and enhancements.

### Related content

- [Coupled magnetic, structural, and electronic phase transitions in FeRh](#)  
L H Lewis, C H Marrows and S Langridge
- [Structural evidence for stabilized ferromagnetism in epitaxial FeRh nanoislands](#)  
M Loving, F Jimenez-Villacorta, B Kaeswurm *et al.*
- [Magnetization reversal and confinement effects across the metamagnetic phase transition in mesoscale FeRh structures](#)  
Jon Ander Arregi, Michal Horký, Kateina Fabianová *et al.*

### Recent citations

- [Special issue on caloric materials](#)  
Luís Mañosa and Antoni Planes



**IOP | ebooks™**

Bringing you innovative digital publishing with leading voices to create your essential collection of books in STEM research.

Start exploring the collection - download the first chapter of every title for free.

# Strain-tuning of the magnetocaloric transition temperature in model FeRh films

M G Loving<sup>1,6</sup>, R Barua<sup>1,5</sup>, C Le Graët<sup>2,7</sup>, C J Kinane<sup>3</sup>, D Heiman<sup>4</sup>,  
S Langridge<sup>3</sup>, C H Marrows<sup>2</sup> and L H Lewis<sup>1,5</sup>

<sup>1</sup> Department of Chemical Engineering, Northeastern University, Boston, MA 02115, United States of America

<sup>2</sup> School of Physics and Astronomy, University of Leeds, Leeds LS2 9JT, United Kingdom

<sup>3</sup> ISIS, Harwell Science and Innovation Campus, Science and Technology Facilities Council, Rutherford Appleton Laboratory, Didcot, Oxon, OX11 0QX, United Kingdom

<sup>4</sup> Department of Physics, Northeastern University, Boston, MA 02115, United States of America

<sup>5</sup> Department of Mechanical Engineering, Northeastern University, Boston, MA 02115, United States of America

E-mail: [lhlewis@northeastern.edu](mailto:lhlewis@northeastern.edu)

Received 9 June 2017, revised 20 November 2017

Accepted for publication 24 November 2017

Published 15 December 2017



## Abstract

The chemically ordered B2 phase of equiatomic FeRh is known to absorb or evolve a significant latent heat as it traverses its first-order phase transition in response to thermal, magnetic, and mechanical drivers. This attribute makes FeRh an ideal magnetocaloric material testbed for investigation of relationships between the crystalline lattice and the magnetic spins, which are especially experimentally accessible in thin films. In this work, epitaxial FeRh films of nominal 30 nm and 50 nm thicknesses with out-of-plane *c*-axis orientation were sputter-deposited at high temperature onto (001)-MgO or (0001)-Al<sub>2</sub>O<sub>3</sub> substrates and capped with Al, Au, Cr, or W after *in situ* annealing at 973 K to promote CsCl-type chemical order. In this manner a controlled strain state was invoked. Experimental results derived from laboratory and synchrotron x-ray diffraction combined with magnetometry indicate that the antiferromagnetic (AF)—ferromagnetic (FM) magnetostructural phase transformation in these films may be tuned over an ~50° range (373 K–425 K) through variation in the *c/a* ratio derived from lattice strain delivered by the substrate and the capping layers. These results supply fundamental information that might be used to engineer the magnetocaloric working material in new system designs by introducing targeted values of passive strain to the system.

Keywords: strained films, FeRh, epitaxial layers

 Supplementary material for this article is available [online](#)

(Some figures may appear in colour only in the online journal)

## 1. Introduction and background

Elucidation of materials pathways that allow inter-conversion of thermal energy with other forms of energy is of both fundamental scientific and applied technological importance. In

particular, materials that undergo thermodynamically first-order magnetic phase changes couple magnetic and thermal energies, providing functionality via the giant magnetocaloric effect (MCE) for solid-state magnetic refrigeration and vibrational and thermal energy harvesting, among other emerging applications [1]. The functional response of such materials originates in very strong orbital-lattice coupling that donates large, coincident changes in magnetic ( $\Delta S_{\text{magnetic}}$ ) and lattice ( $\Delta S_{\text{lattice}}$ ) entropies that may be transformed into absorption

<sup>6</sup> Current address: Northrop Grumman Corporation, Advanced Technology Lab, 1212 Winterson Road, MS3E16 Linthicum, MD 21090.

<sup>7</sup> Current address: AXON<sup>MECHATRONICS</sup> SAS, 103 avenue de Ty-bos, 29556 QUIMPER cedex 9, France.

or evolution of thermal energy, creating a MCE [2, 3]. The intrinsically strong crystallographic—magnetic lattice interaction in magnetostructural materials implies that first-order magnetic phase transitions, and their associated functional responses, may be driven via a plurality of intensive thermodynamic variables such as magnetic field  $\mu_0 H$ , pressure  $P$ , strain  $\sigma$ , and temperature  $T$ , or combinations thereof, creating a rich multi-dimensional phase space for optimization of the magnetocaloric response. Here we report the structural and thermomagnetic character of epitaxial FeRh films capped with proximal layers that donate a compressive or tensile strain to the lattice. Depending on the nature of the strain, it is found that the magnetostructural transition temperature of FeRh may be tuned over an approximate  $50^\circ$  range (373 K–425 K). These results provide fundamental knowledge concerning strain-tuning of magnetocaloric materials to aid in the design of next-generation thermal management technologies, including magnetic refrigeration [4].

Ideally, materials for energy-relevant magnetocaloric applications should exhibit an abrupt first-order magnetic phase transition with a tunable, near-room-temperature transition temperature. Magnetic refrigerators that utilize active magnetic regeneration (AMR) technology typically require a multi-layered architecture of working materials, each with a disparate but relatively close magnetic transition temperature, to realize a large working temperature span. Further, magnetocaloric materials should have a moderate heat capacity fostering a large temperature exchange with the working medium, and they should exhibit minimal volumetric and thermomagnetic hysteresis enabling their mechanical integrity over thousands of thermal cycles. Finally, these materials should not be reactive with the working medium and should be comprised of earth-abundant, accessible and economical elements. Among the small family of materials with room-temperature magnetostructural transitions, the chemically ordered FeRh compound with the CsCl-type structure (B2 Strukturbericht designation) provides an exceptional magnetocaloric response that has the potential to satisfy all of the above criteria, save for the last one [5]. However, it may be noted that magnetic hysteresis can be a feature of many magnetocaloric materials, but can be managed through careful engineering of the barriers to equilibrium phase nucleation.

The FeRh B2-type compound, depicted in figure 1, transforms from a G-type antiferromagnetic (AF) state to a ferromagnetic (FM) state on heating through the critical transition temperature  $T_t \approx 380$  K [6] and is accompanied by an isotropic 1% volume expansion [7, 8] in bulk samples. Associated with this first-order phase transition is a decrease in resistivity by typically a factor of 2 [1], a significant drop in the ordinary Hall coefficient [9], and a large entropy release [5, 10]. This large entropy release is transformed into a giant adiabatic temperature change of  $\Delta T_{ad} = 12.9$  K under an applied field of 2 T [5, 10] granting FeRh the record adiabatic temperature change per Tesla for any room temperature magnetocaloric material. This attribute has attracted significant interest for the application of FeRh in niche or micromagnetocaloric systems.

FeRh was first reported in 1938 by Fallot [11, 12]; since the original work of Fallot, several reports have shown that

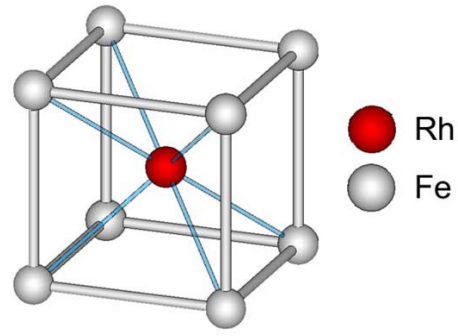


**Figure 1.** Depiction of the CsCl- (B2)-type crystal structure of  $\alpha'$ -FeRh.

bulk FeRh undergoes a first-order magnetic transition from AF to FM order with increasing temperature at  $T_t \sim 350$  K [6, 7, 13–15]. As the temperature is further increased to a temperature above the Curie temperature the FeRh system then undergoes the usual second-order, FM–paramagnetic (PM) transition [8, 16] at  $T_C \sim 670$  K. The AF–FM transformation in bulk FeRh is typically accompanied by a thermal hysteresis of approximately 10 K [8, 17–19]. Neutron diffraction studies of the magnetic moments associated with the Fe and Rh atoms have shown that FeRh in the FM state has a magnetic moment of  $3.04 \mu_B$  per Fe atom and  $\sim 1 \mu_B$  per Rh atom [19, 20]. At room temperature—in the AF state—bulk FeRh has zero net magnetic moment; the magnetic moments associated with the Fe atoms are antiferromagnetically ordered with magnetic moments of  $3.3 \mu_B$  per Fe atom while there is a magnetic moment of zero  $\mu_B$  per Rh atom [1, 19–25].

It has been documented in FeRh systems (both bulk and thin film forms) that the magnetostructural transition is very sensitive to synthesis conditions [26–28], detailed composition [16, 29–42], magnitude of the applied magnetic field [16, 43] and to pressure (strain) conditions [10, 33, 41, 44–48]. While the effect of pressure on the onset of  $T_t$  in bulk FeRh systems has been well documented [33], strain effects in thin films due to epitaxial film/substrate clamping have not been as widely studied [43, 49, 50]. Clamping of the FeRh film is anticipated to result in a structural transformation which is constrained in the in-plane (lateral) direction, relative to the isotropic expansion of bulk FeRh [27, 39, 51]. Further, thin film forms of FeRh often exhibit a broad thermomagnetic transition over many tens of degrees and a remanent FM phase, manifest as a positive remanence, retained in the bulk AF-regime. The exact origin of this remanent FM phase is currently unknown; however, many authors have attributed the retained FM layer to compositional fluctuations or strain at the film interfaces [49, 52, 55, 56]. A reported ‘colossal’ asymmetric magnetothermal hysteresis in mesoscale (sub-micron) patterned FeRh films has been attributed by Uhlír *et al* [53] to a large intrinsic difference in the exchange length characterizing the FM and AF phases. Recently, x-ray photoemission electron microscopy (XPEEM) imaging of the FeRh first-order phase transformation clearly exhibits FM phase nucleation and growth in the FeRh thin film system [52, 54]. Further, these studies indicate that the nucleation of the FM phase upon heating through the AF–FM first-order phase transformation occurs at many

nucleation sites with random magnetic domain orientation. These XPEEM studies indicate that in the nominal AF regime there is some remnant FM phase retained near the interfaces. This conclusion is in agreement with results obtained from earlier studies of data derived from x-ray magnetic circular dichroism (XMCD) [55] and polarized neutron reflectivity (PNR) [56] experiments, where the remanent FM layer is attributed to strain at the substrate-film interface.

The magnetostructural transformation temperature in bulk FeRh has been shown to increase with increasing compressive strain [33, 41, 45, 46] and decrease with tensile strain [10]. Strain effects in FeRh films have been previously studied by measuring the magnetic and structural properties before and after delamination from the substrate [44]. In that study, the magnetostructural transition temperature of the delaminated FeRh films approached bulk-like values, confirming that strain can indeed modify the magnetostructural character. Other studies have connected the observed  $T_t$  shift in films with a distortion of the FeRh film crystal lattice: it is hypothesized in the literature that an increase in the in-plane lattice constants, induced by tensile strain exerted on the FeRh film layer, stabilizes the FM phase leading to a lower  $T_t$  [57], while a lattice expansion of epitaxially clamped FeRh is hindered in the lateral direction due to a constrained lattice, relative to the out-of-plane direction [31, 41, 51, 58]. To date, no direct measurements of the evolution of the lattice parameter of bulk FeRh to changes in pressure have been reported.

## 2. Experimental rationale and design

This work seeks to probe and better understand the effects of strain on the magnetostructural transition of FeRh, which serves as a proxy for other potential room-temperature MCE materials. Analyses of earlier work concerning correlations between strain/pressure and magnetism in bulk FeRh, summarized in the previous section, have inspired this current work. In contrast to bulk forms, thin film forms of FeRh are amenable to passive and convenient strain variation through appropriate matching of substrate and/or capping layer materials. FeRh in thin film form is reported to display magnetic and structural features which are consistent with those of bulk FeRh (i.e. the AF-FM transformation with an accompanying lattice expansion upon heating). However, anisotropic strain which results from epitaxial film/substrate clamping can lead to the emergence of variations in the transformation character of FeRh thin films, relative to that manifest in bulk FeRh [55, 56, 58, 59]. In particular, FeRh film/substrate clamping may result in a deformation which is constrained in the in-plane (lateral) direction, relative to the isotropic expansion of bulk FeRh, and thus lowers the crystallographic symmetry from the original cubic designation [39, 49, 51]. The convention adopted here is the lattice  $a$ -parameter refers to the in-plane lattice parameter of the films, while the lattice  $c$ -parameter refers to the out-of-plane film parameter.

It is clear that the magnetostructural attributes of a FeRh may be dramatically affected by strain delivered to the lattice. This strategy opens another route, besides doping [42],

for adjusting the transition temperature of magnetocaloric materials. In this work, the FeRh lattice is synthesized in thin film form and is strained by the substrate and a proximal capping layer. The lattice parameters and magnetostructural phase transition temperatures of well-ordered FeRh epilayer thin films deposited on MgO and Al<sub>2</sub>O<sub>3</sub> substrates, capped with metallic layers of Al, Au, Cr, and W, were investigated. The capping layers were specifically selected to deliver either compressive or tensile stress to the FeRh lattice. While Al and Au are common capping materials for thin film systems, Cr and W were specifically chosen on the basis that they both crystallize in the body-centered-cubic (bcc) structure, the simple lattice on which the B2-structure of FeRh is based. In bulk form the lattice constant for Cr is 0.291 nm, while that for W is 0.316 nm [60], compared to the reference lattice parameter of 0.2988 nm for FeRh in the AF state (0.2997 nm in the FM state [8]). The resulting epitaxial lattice mismatch was hypothesized to give rise to compressive and tensile strains at the FeRh interface for Cr and W, respectively. As the FeRh lattice experiences a lattice expansion from the AF to the FM state with increasing temperature, tensile strain is anticipated to promote the onset of the higher-volume FM state, thereby facilitating the transition, and compressive strain is anticipated to impede the transition upon heating. The magnetic properties of the chosen capping layers are similarly disparate: W is a paramagnet that delivers a tensile strain by virtue of its large Young's Modulus of 411 GPa relative to that of FeRh in the AF state of  $E = 170$  GPa [61, 62]. On the other hand, Cr, with a Young's Modulus of 279 GPa, is a complex antiferromagnet with a bulk Néel temperature of 312 K and exhibits an onset of antiferromagnetism at thickness of 4.2 nm in thin film form [63, 64]. It is the only bcc transition metal with a lattice constant smaller than FeRh, and thus it was our only choice as a metal to apply compressive strain. While the FeRh magnetostructural transition might be influenced by the magnetic character of Cr, the main effect of the Cr layer is considered to be mechanical.

The strain delivered epitaxially by a given capping layer to the FeRh film may be quantified by the lattice strain  $f_m$  due to lattice mismatch as:

$$f_m = \frac{a - a_0}{a_0} \quad (1)$$

where  $a$  is the experimentally determined (in-plane or lateral) film lattice parameter and  $a_0$  is the unstrained analogous lattice parameter value of the capping layer. Strained films have lattice parameters that can be larger or smaller than bulk values; a positive value of  $f_m$  indicates tensile strain while a negative value of  $f_m$  indicates compressive strain, relative to the bulk lattice.

The magnitude of strain-related effects is anticipated to be larger in FeRh film systems that are strained throughout the entire film thickness by the substrate and capping layer. While the film may be strained elastically at the epitaxial capping layer/film interface to adopt an interatomic spacing close to that of these proximal components, at a critical thickness the strain is relieved by the introduction of dislocations into the film. At distances within the film greater than  $d_c$  this

strain is largely eliminated. The critical thickness  $d_c$  may be estimated as

$$d_c = \frac{a}{2f_m} \quad (2)$$

where  $a$  is the experimentally determined lattice parameter and  $f_m$  is the lattice mismatch strain as defined earlier [65]. This criterion allows an estimate of the effectiveness of the strain in changing the lattice attributes.

### 3. Experimental details

Single-crystal FeRh thin films were deposited and capped with a variety of elemental metallic layers and were subjected to structural and magnetic probes to assess their magnetostructural attributes.

Thin films of the B2-ordered FeRh compound were synthesized using dc magnetron sputtering from a target of composition Fe<sub>47</sub>Rh<sub>53</sub> onto single-crystal MgO (001) or (0001)-type Al<sub>2</sub>O<sub>3</sub> substrates. Nominal film thicknesses were 50 nm or 30 nm, and the film systems are denoted in this work as (cap)/FeRh/(substrate). The film substrates were rinsed with isopropanol, mounted in the sputter chamber, and annealed at 973 K for 12 h at a pressure of 10<sup>-6</sup> Torr. After annealing, the bare substrates were cooled to 873 K and liquid nitrogen was introduced into the cold trap of the sputter chamber to improve the vacuum to 10<sup>-7</sup> Torr. Prior to deposition, the FeRh targets were pre-sputtered so that a steady state composition for deposition was achieved and the deposited film composition roughly matched the target compositions. The film growth was performed at a substrate temperature of 870 K using an Ar/4% H<sub>2</sub> sputter gas at a pressure of 4 × 10<sup>-3</sup> Torr and a DC power of 6 W, which yields a slow growth rate of 0.04 nm/s, as calibrated by *ex situ* x-ray reflectivity (XRR) measurements (data not provided). After deposition of the desired film thickness of 50 or 30 nm, the sample temperature was increased to 973 K and the films were annealed for 1 h to promote CsCl-type chemical-ordering. The samples were then cooled *in situ* in order to minimize any interdiffusion of subsequently deposited caps with the FeRh layer. The epitaxial strain layers of Cr (nominally 5 nm) or W (nominally 8 nm) were covered by a nominally 2 nm thick Al capping layer, deposited at  $T = 370$  K. After a successful deposition, the films typically had a shiny surface indicating achievement of a metallic character. Utilization of the two different substrate types allowed variation of the crystallographic orientation and distortion of the deposited film. The FeRh unit cell was found to be oriented such that lattice planes of FeRh are aligned in the [001] and [111] directions on MgO and Al<sub>2</sub>O<sub>3</sub>, respectively. Specifically, the FeRh/MgO films were tetragonally distorted while the FeRh/Al<sub>2</sub>O<sub>3</sub> films were trigonally distorted from the prototypical cubic FeRh unit cell. In this work the unstrained lattice parameter of FeRh, in the AF bulk cubic structure is taken as  $a_0 = 0.2988$  nm Å [8].

The film layer thickness, interfacial roughness and crystal structure were confirmed by the x-ray scattering techniques of XRR and x-ray diffraction (XRD). Specular XRR measurements were performed and fitted using the open source GenX

software [66]. In accordance with the GenX user manual, the error bars for the XRR data are estimated as a 5% increase of the optimal figure of merit; the error values provided in the next section were taken directly from the output of the fits achieved with the GenX program.

Employing the above-described procedure, the thicknesses and interfacial roughnesses of the FeRh and the capping film layers were determined by fitting the XRR data with the simplest model to provide a good fit to the experimental data, with resultant low and very favorable figures of merit. Room-temperature crystal structure data used to confirm attainment of the desired phase were provided by laboratory-based XRD to determine the FeRh lattice parameters and degree of strain. Additionally, the chemical order parameter  $S$  that quantifies the degree of perfection of the atomic arrangement on the B2 lattice sites was evaluated in the manner of our earlier work [9]. The in-plane ( $a$ ) and out-of-plane ( $c$ ) lattice parameters were determined on the Al-capped films, while only out-of-plane lattice parameters were studied on films capped with Cr, W or Au. In this work either a PANalytical X'Pert PRO MPD Theta-2Theta System or a Bruker Model D8 Discover diffractometer (both utilizing Cu-K<sub>α</sub> radiation with a wavelength  $\lambda = 0.1541$  nm) was utilized for laboratory-based structural characterization. These diffractometers employ a Bragg–Brentano configuration that probes crystallographic planes orthogonal to the x-ray scattering vector; thus, out-of-plane lattice parameters could be obtained from appropriately scattering planes in the single-crystal epifilms. In-plane diffraction data were obtained on the Al-capped films by physically rotating the film sample or by introducing an offset to the theta arm of the goniometer. Values for the in-plane lattice parameters of the Cr-, W- and Au-capped films were calculated from the out-of-plane lattice parameter values, assuming a conserved FeRh unit cell volume of  $V = 0.0266$  nm<sup>3</sup>. This assumption is validated upon calculation of the FeRh unit cell volume using values reported in the literature from a selection of sources [43, 49, 50, 56, 67], with results provided in the supplementary material section ([stacks.iop.org/JPhysD/51/024003/mmedia](http://stacks.iop.org/JPhysD/51/024003/mmedia)). To study the FeRh films as they traversed the magnetostructural transition, *in situ* temperature-dependent XRD studies were carried out at the National Synchrotron Light Source (NSLS) at Brookhaven National Laboratory, Upton, New York, using the facility at Beamline X22C equipped with a Franke and Heydrich 6-circle diffractometer. Incident x-ray photon energies of 10 keV or 11 keV ( $\lambda = 0.1238$  nm or 0.1127 nm) were employed to examine the films upon heating and cooling through the magnetostructural transformation temperature. Diffraction studies were carried out as a function of temperature while traversing through the magnetostructural transition in the range of 300 K ≤  $T$  ≤ 424 K with 10 K steps. The drift in temperature during data collection was ± 0.2 K. To ensure that no changes had occurred in the FeRh lattice during the thermal cycling, (00 $L$ ) XRD data were collected and compared before and after heating through the transition. The resultant Bragg peaks were indexed to a body-centered tetragonal (BCT) unit cell on the basis of the assumption that epitaxial clamping of the film layer may result in a lattice distortion at the film interfaces. The Bragg

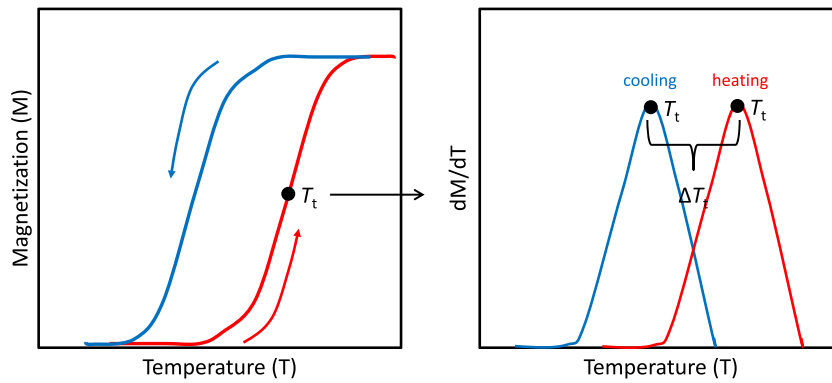


**Figure 2.**  $M(T)$  diagrams showing the methods used for defining the transition temperature,  $T_t$ , and thermal hysteresis width  $\Delta T_t$ . (Left):  $M(T)$  character of the FeRh transition. (Right): derivative transformation of the left side data. Here, the  $T_t$  values are defined as the temperature of the maxima of the derivative curves, at the midpoint of the  $M(T)$  curve.

peaks were fitted with a double pseudo-Voigt fitting function, and were compared to the reported bulk FeRh cubic lattice parameter of 0.2988 nm in the AF phase to obtain an estimate of film strain [8, 43].

The magnetic properties of the films were assessed as they traversed the magnetostructural transition with data derived from superconducting quantum interference device (SQUID) magnetometry in applied fields up to 5 T, in the temperature range  $250 \text{ K} \leq T \leq 600 \text{ K}$ . To collect the magnetic data for  $T \leq 400 \text{ K}$  (as was required for the Cr/FeRh/MgO and W/FeRh/MgO films), a high temperature furnace attachment was installed into the SQUID magnetometer. For these measurements samples were vacuum-sealed in vitreous silica tubes at a pressure of  $\sim 10^{-6}$  Torr to prevent oxidation. A sweep rate of  $2 \text{ K min}^{-1}$  was employed during measurements. The magnetostructural transition temperature  $T_t$  was determined as the average value of the temperature at which a maximum is obtained in the derivative of magnetization versus temperature  $M(T)$  data with respect to  $T$  as obtained upon heating and cooling, while the width of the thermal hysteresis,  $\Delta T_t$ , is quantified as the difference between the maxima of the derivatives of the heating and cooling  $M(T)$  curves. More precise estimates of  $T_t$  and  $\Delta T_t$  are obtained from Gaussian curve fits to the  $\frac{\partial(M(T))}{\partial T}$  curves; these definitions are illustrated in figure 2 for enhanced clarity. The transition temperatures were corrected for the shift due to the magnitude of the applied field as  $-0.8 \text{ K/kOe}$  [43]. The transition temperatures and transition widths determined in this manner have estimated errors on the order of 1%. All of the magnetic data were collected with the magnetic field applied parallel to the film plane; no demagnetization corrections were applied.

## 4. Results and discussion

Data derived from structural and magnetic probes of films of FeRh capped with thin layers of Al, Au, Cr, and W provide a picture of the relationship between the magnetostructural transition temperature and the degree of the film lattice distortion. As denoted above, the convention applied to describing the capped FeRh films is X/FeRh/Y where X corresponds to the capping layer material and Y corresponds to the substrate material.

Attainment of smooth and well-correlated film interfaces was confirmed through analysis of the XRR data that present pronounced Kiessig fringes, which arise from the interference of x-ray beams that reflect from the various interfaces in the layer stack; typical results are shown in figures 3(a) and (b), with best-fit parameters for the multilayer structures shown in table 1. The fact that a portion of the capping layer will have oxidized and self-passivated once the sample is exposed to air is accounted for in the model. The depth profiles resulting from these fits indicate that film interfaces are sharp, with roughnesses typically smaller than 0.4 nm at the substrate interface and of the order of 0.5 nm at the capping interface; these roughness values in fact contain contributions from actual topographical roughness and from interdiffusion between the layers.

As very little interdiffusion of the FeRh film with the oxide substrates is expected, the substrate roughness values give a good estimate of the true topographical roughness. Sputtering methods produce very conformal layers, and this roughness is likely to be reproduced at the capping layer; thus the degree of interdiffusion at the film/cap interfaces is expected to be limited to only 0.1–0.2 nm.

### 4.1. Structural results

The FeRh films were confirmed to be single crystal epilayers that were slightly distorted from the prototypical cubic CsCl unit cell, thereby providing  $c/a$  parameters that differ from unity. The films were found to have no additional phases present other than FeRh in the XRD patterns, and the presence of the (001) superstructure peak indicates achievement of B2-type chemical order. The FeRh films deposited onto the (001)-oriented MgO substrate have a film-substrate orientation relationship of (001)-FeRh on (001)-MgO while the FeRh film deposited onto (0001)- $\text{Al}_2\text{O}_3$  substrate has an orientation relationship of (111)-FeRh on (0001)- $\text{Al}_2\text{O}_3$ . The chemical-order parameters ( $S$ ) are determined to be in the range  $S \sim 0.85\text{--}0.89$  for films deposited on MgO substrates, confirming a high degree of chemical order. While it was not possible to obtain the order parameter for the film deposited on the  $\text{Al}_2\text{O}_3$  substrate due to equipment limitations, it is presumed that it also possess a high degree of chemical order. Structural results for all of the films are summarized in table 1. It is interesting to

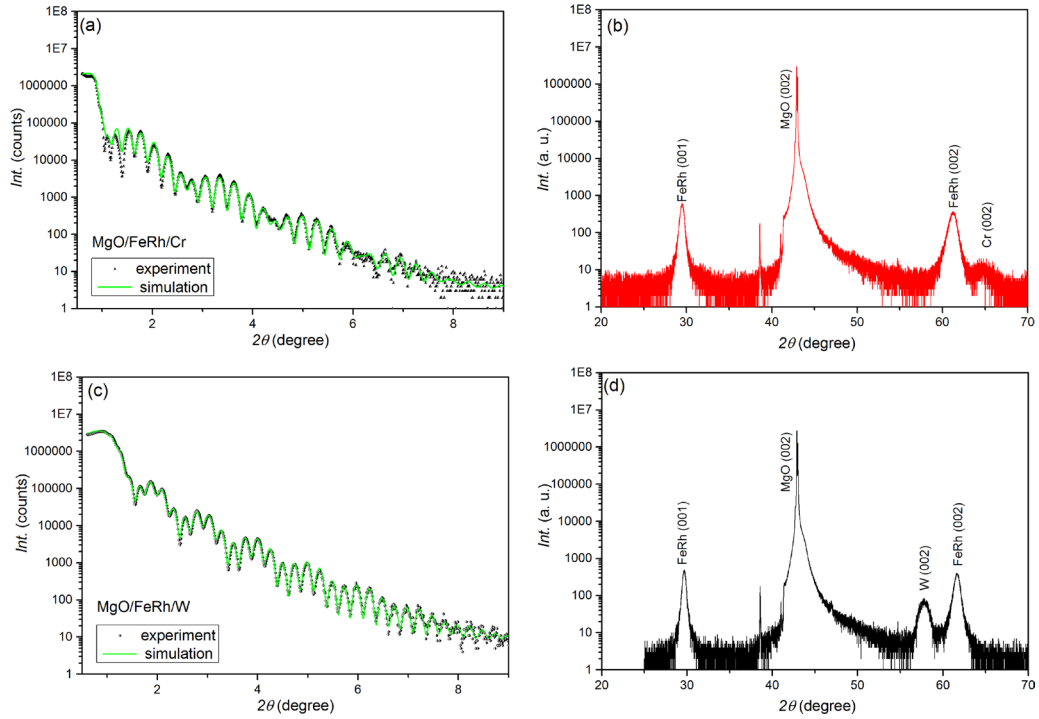


**Figure 3.** Examples of typical laboratory x-ray diffraction data obtained from the capped FeRh films: (a) XRR results of the Cr/FeRh/MgO film; (b) Full high-angle  $\theta/2\theta$  scan of the Cr/FeRh/MgO film; (c) XRR results of the W/FeRh/MgO film. (d) Full  $\theta/2\theta$  scan of the W/FeRh/MgO film. The peak observed at the position  $2\theta = 39^\circ$  is attributed to the MgO substrate resulting from incompletely filtered  $\text{Cu K}\beta$  radiation.

**Table 1.** Fitting parameters of the fits to the XRR data for the FeRh films of this study. Note the complete oxidation of the Al cap in the Al/FeRh/ $\text{Al}_2\text{O}_3$  film stack.

Sample	Layer	Thickness (nm)	Interfacial Roughness (nm); errors in roughness typically less than 0.5%
Al/FeRh/MgO	$\text{AlO}_x$ (passivation layer)	$2.80 \pm 0.02$	0.910
	Al	$0.15 \pm 0.02$	0.910
	FeRh epilayer	$50.43 \pm 0.03$	0.4400
	MgO (substrate)	$\infty$	0.430
Al/FeRh/ $\text{Al}_2\text{O}_3$	$\text{AlO}_x$ (passivation layer)	$2.5 \pm 0.1$	1.010
	Al	$0.000 \pm 0.0009$	0.00 (fully oxidized cap)
	FeRh epilayer	$51.01 \pm 0.03$	0.4500
	$\text{Al}_2\text{O}_3$ (substrate)	$\infty$	0.4500
Au/FeRh/MgO	Au	$3.50 \pm 0.05$	0.7
	FeRh epilayer	$45.20 \pm 0.05$	0.7
	MgO substrate	$\infty$	0.1
Al/Cr/FeRh/MgO	$\text{AlO}_x$ (passivation layer)	$3.00 \pm 0.08$	1.7
	Cr	$5.00 \pm 0.08$	0.43
	FeRh epilayer	$27.05 \pm 0.06$	0.56
	MgO (substrate)	$\infty$	0.32
Al/W/FeRh/MgO	$\text{AlO}_x$ (passivation layer)	$3.00 \pm 0.08$	1.7
	W	$8.00 \pm 0.08$	0.48
	FeRh epilayer	$27.05 \pm 0.06$	0.56
	MgO (substrate)	$\infty$	0.32

note that the lattice parameters of the Cr and W capping layers, as calculated from the (002) Bragg peak positions, are significantly distorted from their bulk values. The lattice parameter of the Cr cap is calculated as  $a = 0.3189 \pm 0.006$  nm, compared to the bulk value of 0.291 nm, while that for the W cap is determined as  $a = 0.2887 \pm 0.0002$  nm, compared to its bulk value

of 0.316 nm. These changes clearly indicate a reciprocal deformation of the lattice between the FeRh and capping layers. The determined film thicknesses presented in table 1 are all larger than the critical thicknesses (equation (2)), listed in table 3, for all films investigated; thus it is confirmed that the film strain does not become relieved from the introduction of dislocations.

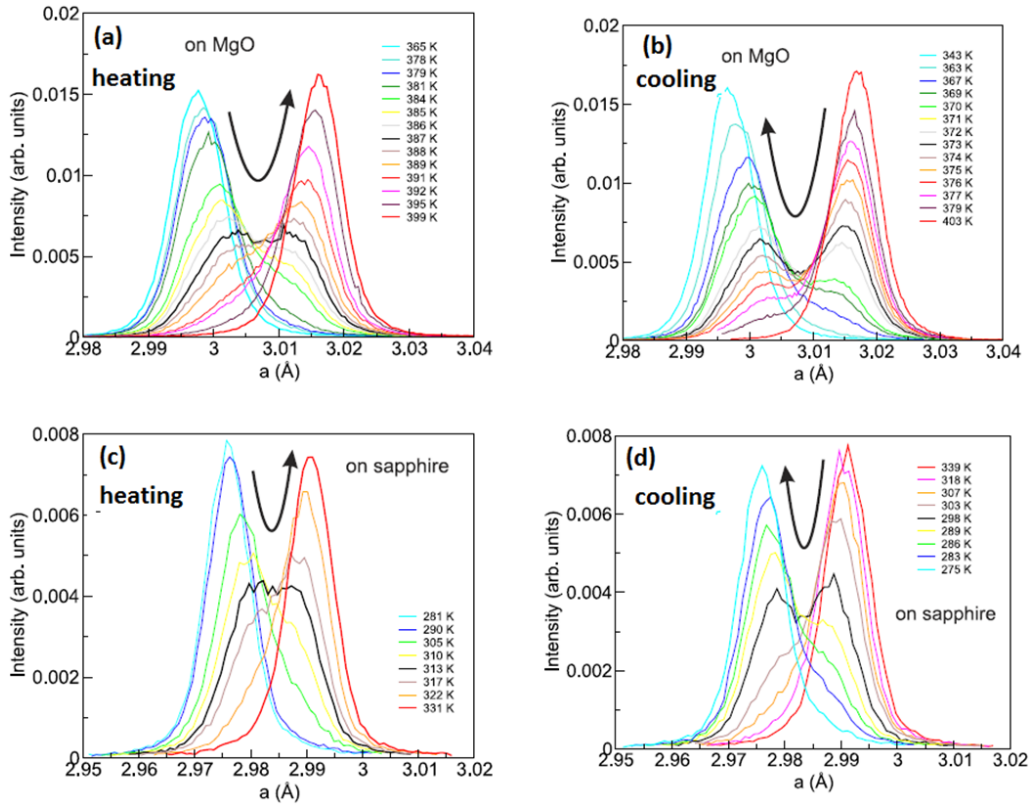


**Figure 4.** Temperature-dependent XRD patterns collected at beamline X22C at the NSLS. Data collected upon (a) heating and (b) cooling through  $T_1$  of the Al/FeRh/MgO (004) Bragg reflections and (c) heating and (d) cooling through the Al/FeRh/Al<sub>2</sub>O<sub>3</sub> (222) Bragg reflection. Figures (a) and (b) are reprinted from [68], with the permission of AIP Publishing.

**Table 2.** In- and out-of-plane lattice parameters ( $a$ -parameters and  $c$ -parameters, respectively), strain %, estimate of the lattice distortion ( $c/a$ ), unit cell volume and chemical order parameters for the FeRh films of this study. Note that the in-plane lattice parameters for the Cr, W, and Au films were estimated assuming a conserved unit cell volume.

Film system	$a$ -parameter (Å)/strain (%)	$c$ -parameter (Å)/strain (%)	$c/a$ ratio	Unit cell volume (nm <sup>3</sup> )	$S$ (order parameter)
Al/FeRh/Al <sub>2</sub> O <sub>3</sub>	3.003/+ 0.502	2.991/+ 0.10	0.9960	0.0270	—
Al/FeRh/MgO	2.984/− 0.130	2.995/+ 0.23	1.0037	0.0266	0.85
Au/FeRh/MgO	2.986/− 0.081	2.992/+ 0.13	1.0021	0.0266	0.86
Cr/FeRh/MgO	2.969/− 0.627	3.025/+ 1.238	1.0188	0.0266	0.89
W/FeRh/MgO	2.978/+ 0.636	3.007/+ 0.636	1.0097	0.0266	0.83

Structural aspects of the magnetostructural phase transformation in the FeRh films are informed by results from synchrotron-based temperature-dependent x-ray diffraction. Figures 4(a)–(d) shows representative temperature-dependent Bragg reflections for the Al/FeRh/MgO and Al/FeRh/Al<sub>2</sub>O<sub>3</sub> films upon heating and cooling through the transformation; all films studied displayed analogous behavior. The films display a two-phase character, as anticipated for a first-order phase transition, at temperatures in the intermediate regime of the transition. It is evident that the Bragg peak separation, reflecting the lattice spacing of the two phases, is larger on cooling than on heating. This asymmetry is consistent with the difference in the kinetics of the magnetostructural phase transition in this material [68].

As described in section 2, these data were analyzed using equation (1) to produce the values for the lattice misfit and strain for the films, which are documented in tables 2 and 3.

#### 4.2. Magnetic results

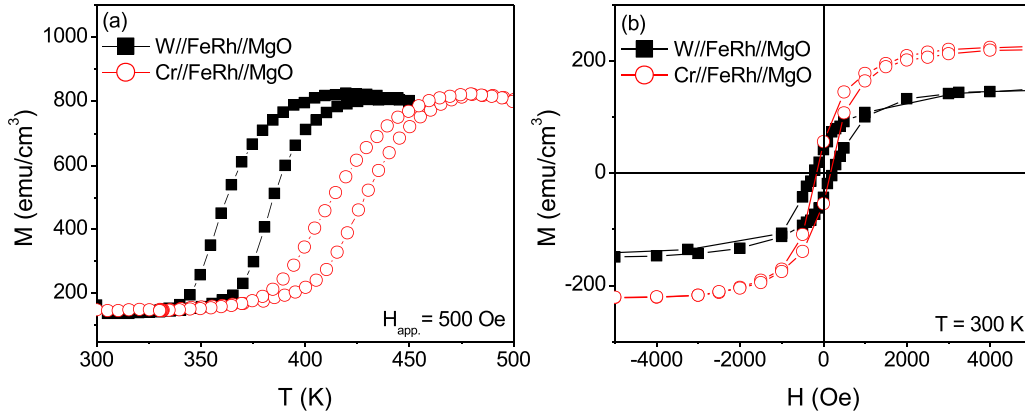
The magnetization of all films exhibited a low-moment to high-moment progression with increasing temperature, identified as the AF–FM phase transition. (The low but finite magnetization present at low temperature is attributed to the retained FM phase, as described in section 2.) Representative of the magnetic behavior of all the studied samples, figure 5 displays  $M$ – $T$  and  $M$ – $H$  data obtained from the Cr- and the W-capped FeRh/MgO films.

The W-capped film has a transition temperature  $T_1 \sim 380$  K, with a temperature hysteresis of about 34 K. A portion of retained ferromagnetism, approximately 144 emu cm<sup>−3</sup>, is noted at room temperature (in the nominal AF state). The transition temperature of the Cr-capped film is increased up to 425 K with a temperature hysteresis of about 25 K and a retained FM fraction of 221 emu cm<sup>−3</sup>. The saturation

**Table 3.** Information pertaining to the lattice misfit ( $f_m$ ) and critical thickness ( $d_c$ ) of films using the bulk lattice parameter value of FeRh (taken as  $a = 2.988 \text{ \AA}$  in the AF state (8)) and literature values for the additional lattice types.

Component	Bulk component $a$ -lattice parameter/lattice type	Lattice misfit ( $f_m$ ), %	Calculated critical thickness $d_c$ (nm)	Strain type
Al <sub>2</sub> O <sub>3</sub> substrate	4.785 $\text{\AA}$ /HCP	-0.3012	49.6	Tensile
MgO substrate	4.212 $\text{\AA}$ /FCC (NaCl-type)	+0.3347	45.3	Compressive
Al capping layer	4.050 $\text{\AA}$ /FCC	-4.1499	3.6	Tensile
Au capping layer	4.080 $\text{\AA}$ /FCC	-3.4806	4.3	Tensile
Cr capping layer	2.880 $\text{\AA}$ /BCC	+3.6144	4.1	Compressive
W capping layer	3.160 $\text{\AA}$ /BCC	-5.7536	2.6	Tensile

HCP = hexagonal close-packed; FCC = face-centered cubic; BCC = body-centered cubic

**Figure 5.** Magnetization data collected as a function of (a) temperature ( $H_{app} = 500 \text{ Oe}$ ) and (b) applied magnetic field ( $T = 300 \text{ K}$ ) for the Cr/FeRh/MgO and W/FeRh/MgO films.**Table 4.** Determined magnetostructural transition temperatures of the films of this study. The transition temperatures are determined as described in section 4, and the amount of retained FM phase is quantified as the fraction of the saturation magnetization  $M_S$  remaining at  $T = 300 \text{ K}$ .

Film System	Saturation magnetization after completed transition to FM state (emu/cc)	Transition temperature $T_t$ (K, heating) at applied field	$T_t$ (K, heating) extrapolated to zero applied field	Width of transition $\Delta T_t$	Retained FM component in AF state (%) at $T = 300 \text{ K}$
Al/FeRh/Al <sub>2</sub> O <sub>3</sub>	876	349 (@ 30 kOe)	373	37	9.0
Al/FeRh/MgO	876	390 (@ 30 kOe)	414	26	7.3
Au/FeRh/MgO	1250	394 (@ 0.1 kOe)	393	30	5.0
Cr/FeRh/MgO	869	425 (@ 0.5 kOe)	425	25	25.9
W/FeRh/MgO	869	380 (@ 0.5 kOe)	380	34	16.6

moments in the (high-temperature) FM state are identical for both films at  $869 \text{ emu cm}^{-3}$ . Table 4 provides a summary of the magnetostructural transition temperatures of the films of this study. The larger percentage of retained FM component in the AF state documented for the Cr- and W-capped samples is correlated with their reduced thickness relative to those of the other samples, as quantified in table 1.

Overall, the structural and magnetic data presented here allow determination of the relationship between the magnetostructural transition temperature  $T_t$  and the degree of the film lattice distortion, allowing the capability of strain-tuning  $T_t$ . Relationships between the in-plane lattice constant, the out-of-plane lattice constant, the FeRh unit cell volume, the degree of film lattice distortion ( $c/a$ ) and the AF-FM transition temperature (evaluated upon heating through the transition) have been developed by combining information from

the  $M(T)$  results and measured lattice parameters; these values have been normalized to  $H_{app} = 0$  assuming a field sensitivity to applied magnetic field of  $-0.8 \text{ kOe/K}$  [14, 43]. These data are compared with values of these parameters derived from both bulk and thin film studies, as reported in the literature presented in section 2, and results from these analyses are graphed in figures 6 and 7.

The crystal lattice of bulk FeRh under uniaxial pressure conditions will experience a reduced symmetry but is anticipated maintain a conserved unit cell volume. Nikitin and coworkers [69] found that  $T_t$  decreases with increased tensile stress applied to polycrystalline FeRh. This scenario contrasts with the results of Wayne [33] who reported that increased hydrostatic pressure delivered to FeRh alloys increases the magnetostructural transition temperature. These contrasting results must be attributed the high degree of sensitivity of

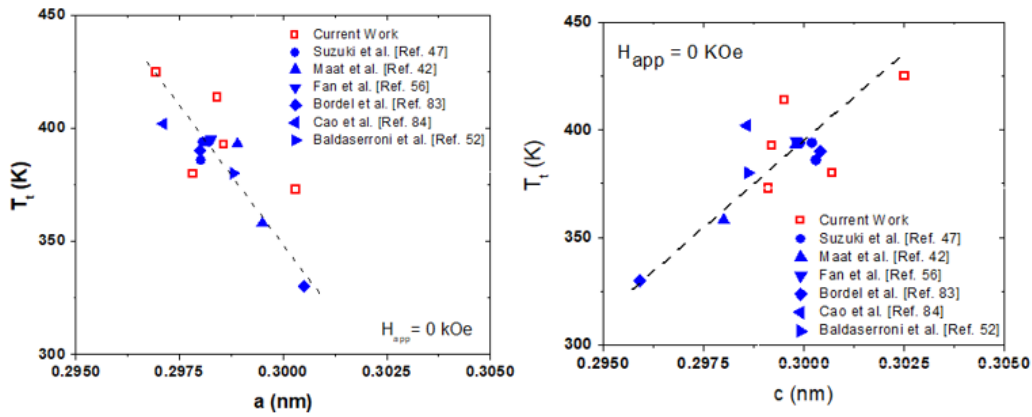


**Figure 6.** Dependence of the magnetostructural transformation temperature ( $T_t$ ) of thin film and bulk FeRh systems as a function of (left) in-plane lattice parameters and (right) out-of-plane lattice parameter. The dotted lines are guides for the eye.

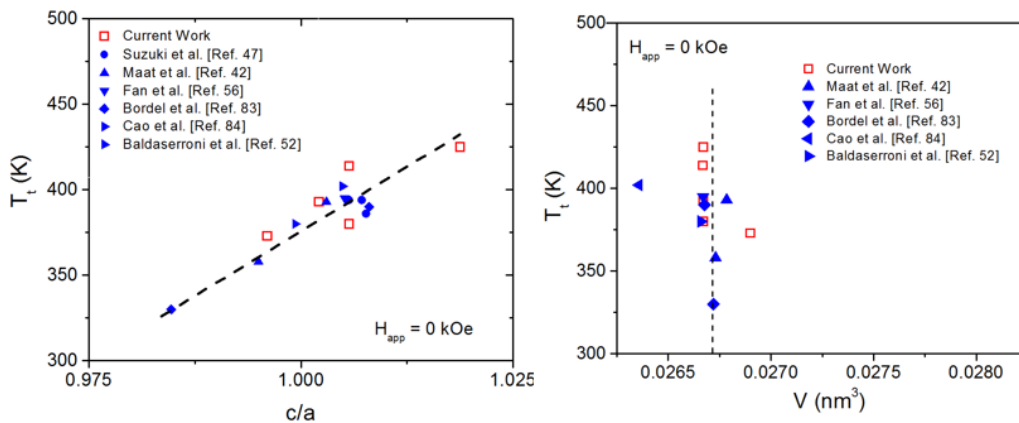


**Figure 7.** Dependence of the magnetostructural transformation temperature ( $T_t$ ) of thin film and bulk FeRh systems as a function of (left) film lattice distortion ( $c/a$ ) and (right) unit cell volume ( $V$ ). The dotted lines are guides for the eye.

the magnetic exchange in FeRh to slight changes in the local atomic environments of the Fe and Rh sublattices.

Within this context, the sensitivity of  $T_t$  to changes of FeRh lattice as studied in thin films during the application of strain/pressure was analyzed, with results summarized in figures 6 and 7. In addition to experimental data from this current study, values for the response of  $T_t$  to applied pressure were taken from a selection of literature sources [10, 36, 41, 43, 45, 70]. The left-hand-side graph of figure 6 indicates that  $T_t$  decreases with increasing in-plane lattice parameter, resulting from the application of tensile strain. In this manner the FM phase can be stabilized in the FeRh thin films. This trend is in agreement with that observed for uniaxially loaded bulk FeRh in which  $T_t$  decreases with increased strain magnitudes (delivering increased lattice parameter values). Alternatively, the right-hand-side graph of figure 6 shows that increasing the out-of-plane lattice  $c$ -parameter results in an increased  $T_t$  with a reduced strain sensitivity (reduced slope) of  $T_t$  relative to that found for in-plane lattice parameter changes. This action can stabilize the AF phase, corroborating results reported by Wayne whereby increased hydrostatic pressure (associated with smaller lattice parameters) delivers lower magnetostructural phase transition temperatures. The sensitivity of the magnetostructural phase transformation temperature to changes in the in-plane ( $a$ ) and the out-of-plane ( $c$ ) lattice parameters, of the distorted FeRh, can be estimated

from the slopes of the  $T_t(a)$  and  $T_t(c)$  plots. These values are surprisingly large; specifically, the in-plane sensitivity is found to be  $\frac{dT_t}{da}$  (film)  $\cong -26\,400\text{ K nm}^{-1}$  ( $-2640\text{ K \AA}^{-1}$ ) while the out-of-plane sensitivity is  $\frac{dT_t}{dc}$  (film)  $\cong 16\,000\text{ K nm}^{-1}$  ( $1600\text{ K \AA}^{-1}$ ). Interestingly, the out-of-plane lattice sensitivity to  $T_t$  is only 60% of the in-plane value. Overall, these large values emphasize the incredible sensitivity of the magnetostructural transition to subtle electronic bonding details. The most valuable illustration of the effect of overall lattice distortion (as described by the  $c/a$  ratio) on the AF–FM transformation temperature in FeRh is presented in figure 7 (left) whereby the transition temperature  $T_t$  increases for  $c/a > 1$  and decreases for  $c/a < 1$ . In other words, a lattice distortion of  $c/a > 1$  stabilizes the AF phase while a lattice distortion  $c/a < 1$  stabilizes the FM phase. It is clear from figure 7 (right) that the unit cell volume is roughly conserved at a value of  $V \sim 0.026\text{ nm}^3$  irrespective of the degree of lattice distortion. This result is intuitively satisfying as the lattice is expected to be free to expand or contract in the unconstrained direction, providing contrast to the behavior of bulk FeRh that demonstrates a linear change in unit cell volume with the application of isostatic pressure [33]. The data scatter noted in figures 6 and 7 may be attributed to slight compositional fluctuations and/or deviations from the assumed  $-0.8\text{ K/kOe}$  sensitivity of the transformation. It is also found that no correlations between the lattice distortion (or

strain) of the FeRh films and the retained FM background (present in the  $M(T)$  curves and quantified in table 4) are observed.

These results allow hypotheses to be developed that explain the observed phenomena. Typically, the increased magnetostructural phase transition temperature of bulk FeRh in response to increased hydrostatic pressure is attributed to magnetovolume effects that change the magnetic interactions of the Fe and Rh atoms [33]. However, the strain-induced lattice distortions of the FeRh films are anisotropic. Thus the current results must be attributed to asymmetric interatomic interaction that can lead to either AF or FM phase stabilization. As each Fe atom in the cubic FeRh lattice has six equally spaced Fe nearest neighbors, tensile strain to produce  $c/a < 1$  increases the interatomic distances of four of out of the six Fe atoms to destabilize the AF state, relative to the bulk FeRh. However, compressive strain to produce  $c/a > 1$  (compressive strain) increases the interatomic distance of only two out of the six Fe atoms. This hypothesis is supported by theoretical work [43, 71].

## 5. Conclusions and outlook

The results of this work demonstrate the feasibility of tuning the FeRh magnetostructural phase transition temperature over a wide range by modifying the lattice through the application of strain. While these results were derived from FeRh films capped by a proximal layer, the concept of strain-tuning the phase transition may be extended to other materials with strong spin-lattice coupling that are under consideration for magnetic cooling applications [72–75]. As such, the results reported here have direct relevance for tailoring the MCE in materials through the application of strain. Not only is the magnetic phase transition temperature affected by strain, the details of the magnetic transition are also affected, resulting in anticipated alterations in the total entropy change and thus of the cooling power delivered by the considered material. Indeed, studies of bulk FeRh have shown that pressure can alter both the entropy change and the net refrigeration capacity of FeRh [76, 77]. Furthermore, recent work by Chirkova *et al* [78] noted that variation in the microstructure can play a role in changing the magnetostructural transition temperature of bulk FeRh that had been subjected to systematic heat treatments. They attributed these phenomena to a concomitant variation in stress fields of their multiphase samples, and also remarked on the connection between the MCE and strain in FeRh-based materials.

The ability to tailor the MCE using passive strain may find applicability in new designs of AMR cooling systems. In particular, the need for a multistage architecture of working materials in AMR cooling systems to realize a large cooling span might be satisfied—and simplified—by the incorporation of a single material that is subjected to a specified strain gradient to realize a cascade of magnetic transition temperatures. Inspiration for engineering static strain into magnetocaloric systems may be taken from the field of civil engineering, in which the important engineering material of reinforced concrete (RC) has been perfected and globally utilized [79]. RC is a composite material comprised of components of relatively low tensile strength and ductility that are

combined ('reinforced') with components of higher tensile strength or ductility. The reinforcement of concrete is commonly delivered through the introduction of steel reinforcing bars that may be permanently stressed (in tension), so as to improve the behavior of the final structure under working loads. It may be possible to adapt this type of extrinsic materials design strategy to create new types of efficient magnetic cooling apparatuses that incorporate materials with first-order magnetic phase changes. Such cross-disciplinary concepts of functional materials design are anticipated to extend the impact and adoption of new technologies.

## Acknowledgments

This work was supported by a linked grant through the Materials World Network scheme by the the UK Engineering and Physical Sciences Research Council, Grant No. EP/G065640/1, and National Science Foundation under Grant No. DMR-0908767; support from NSF Grant ECCS-1402738 is also acknowledged. Use of the National Synchrotron Light Source, Brookhaven National Laboratory, was supported by the US Department of Energy, Office of Science, Office of Basic Energy Sciences, under Contract No. DE-AC02-98CH10886. The data associated with this paper are publicly available from the University of Leeds Data Repository at the following URL: <https://doi.org/10.5518/251>.

## ORCID iDs

M G Loving  <https://orcid.org/0000-0003-0812-2638>  
 R Barua  <https://orcid.org/0000-0001-9268-198X>  
 S Langridge  <https://orcid.org/0000-0003-1104-0772>  
 C H Marrows  <https://orcid.org/0000-0003-4812-6393>  
 L H Lewis  <https://orcid.org/0000-0002-6552-3481>

## References

- [1] Lewis L H, Marrows C H and Langridge S 2016 Coupled magnetic, structural, and electronic phase transitions in FeRh *J. Phys. D: Appl. Phys.* **49** 323002
- [2] Pecharsky V K and Gschneidner K A Jr 2005 Magnetocaloric effect *Encyclopedia Condensed Matter Physics* ed F Bassani *et al* (New York: Elsevier) pp 236–44 and references therein
- [3] Tishin A M and Spichkin Y I 2003 *The Magnetocaloric Effect and its Applications* (Boca Raton, FL: CRC Press)
- [4] Staunton J B, Banerjee R, dos Santos Dias M, Deak A and Szunyogh L 2014 Fluctuating local moments, itinerant electrons, and the magnetocaloric effect: compositional hypersensitivity of FeRh *Phys. Rev. B* **89** 054427
- [5] Sandeman K G 2012 Magnetocaloric materials: the search for new systems *Scr. Mater.* **67** 566–71
- [6] Kouvel J S and Hartelius C C 1962 *J. Appl. Phys.* **33** 1343
- [7] de Bergevin F and Muldrew L 1961 *C. R. Acad. Sci.* **252** 1347
- [8] Zakharov A I, Kadomtseva A, Levitin R and Ponyatovskii E 1964 *J. Exp. Theor. Phys.* **46** 1348
- [9] de Vries M A, Loving M, Mihai A P, Lewis L H, Heiman D and Marrows C H 2013 Hall-effect characterization of the metamagnetic transition in FeRh *New J. Phys.* **15** 013008

- [10] Annaorazov M P, Nikitin S A, Tyurin A L, Asatryan K A and Dovletov A K 1996 *J. Appl. Phys.* **79** 1689
- [11] Fallot M 1938 Les Alliages Du Fer Avec Les Metaux De La Famille du Platine *Ann. Phys.* **10** 291–332
- [12] Kushwaha P, Lakhani A, Rawat R and Chaddah P 2009 *Phys. Rev. B* **80** 174413
- [13] Muldawer L and de Bergevin F 1961 *J. Chem. Phys.* **35** 1904–5
- [14] Kouvel J S, Hartelius C C and Lawrence P E 1963 Entropy change *Bull. Am. Phys. Soc.* **8** 54
- [15] Shirane G, Chen C W, Flinn P A and Nathans R 1963 Hyperfine fields and magnetic moments in FeRh system *J. Appl. Phys.* **34** 1044–5
- [16] Kouvel J S 1966 Unusual nature of the abrupt magnetic transition in FeRh and its pseudobinary variants *J. Appl. Phys.* **37** 1257–8
- [17] Thiele J U, Maat S, Robertson J L and Fullerton E E 2004 Magnetic and structural properties of FePt–FeRh exchange spring films for thermally assisted magnetic recording media *IEEE Trans. Magn.* **40** 2537–42
- [18] Ibarra M R and Algarabel P A 1994 Giant volume magnetostriction in the FeRh alloy *Phys. Rev. B* **50** 4196–9
- [19] Zsoldos L 1967 Lattice parameter change of FeRh alloys due to antiferromagnetic–ferromagnetic transformation *Phys. Status Solidi b* **20** K25–8
- [20] Moruzzi V L and Marcus P M 1992 Antiferromagnetic–ferromagnetic transition in FeRh *Phys. Rev. B* **46** 2864–73
- [21] Thiele J-U, Buess M and Back C H 2004 Spin dynamics of the antiferromagnetic–ferromagnetic phase transition in FeRh on a sub-picosecond time scale *Appl. Phys. Lett.* **85** 2857–9
- [22] Chaboy J, Bartolomé F, Ibarra M, Marquina C, Algarabel P, Rogalev A and Neumman C 1999 X-ray magnetic circular dichroism probe of the Rh magnetic moment instability in  $\text{Fe}_{1-x}\text{Rh}_x$  alloys near the equiatomic concentration *Phys. Rev. B* **59** 3306
- [23] Lounis S, Benakki M and Demangeat C 2003 Ferromagnetic stabilization of ordered B2FeRh thin films *Phys. Rev. B* **67** 094432
- [24] Yamada H, Shimizu H, Yamamoto K and Uebayashi K 2006 Structure and magnetism of 3d and 4d transition-metal alloys  $\text{TT}'$  ( $T = \text{Mn, Fe}$  and  $T' = \text{Rh, Pd}$ ) with CuAu-I type ordered structure *J. Alloys Compd.* **415** 31–7
- [25] Lee J S, Vescovo E, Plucinski L, Schneider C M and Kao C C 2010 Electronic structure and magnetic properties of epitaxial FeRh(001) ultrathin films on W(100) *Phys. Rev. B* **82** 224410
- [26] Lommel J M 1969 Role of oxygen in obtaining complete magnetic first order transitions in FeRh films *J. Appl. Phys.* **40** 1466–7
- [27] Kim J W, Ryan P J, Ding Y, Lewis L H, Ali M, Kinane C J, Hickey B J, Marrows C H and Arena D A 2009 Surface influenced magnetostructural transition in FeRh films *Appl. Phys. Lett.* **95** 222515
- [28] Lommel J M 1966 Magnetic and electrical properties of FeRh thin films *J. Appl. Phys.* **37** 1483–4
- [29] Walter P H L 1964 Exchange inversion in ternary modifications of iron rhodium *J. Appl. Phys.* **35** 938–9
- [30] Algarabel P A et al 1996 Magnetostriction and thermal expansion measurements on  $\text{FeRh}_{1-x}\text{Pt}_x$  alloys *J. Appl. Phys.* **79** 4659–61
- [31] Fullerton E E, Riggs K T, Sowers C H, Bader S D, and Berger A 1995 Suppression of biquadratic coupling in Fe/Cr (001) superlattices below the Néel transition of Cr *Phys. Rev. Lett.* **75** 330
- [32] Tu P et al 1969 Mechanism for the first-order magnetic transition in the FeRh system vol 40 pp 1368–9
- [33] Wayne R C 1968 Pressure dependence of the magnetic transitions in Fe–Rh alloys *J. Appl. Phys.* **40** 1368–9
- [34] Baranov N V and Barabanova E A 1995 Electrical resistivity and magnetic phase transitions in modified FeRh compounds *J. Alloys Compd.* **219** 139–48
- [35] Ibarra M R et al 1995 Giant room temperature volume magnetostriction in an FeRhPd alloy *J. Magn. Magn. Mater.* **140–4** 231–2
- [36] Kushwaha P et al 2009 Low-temperature study of field-induced antiferromagnetic-ferromagnetic transition in Pd-doped Fe–Rh *Phys. Rev. B* **80**
- [37] Van Driel J et al 1999 *J. Appl. Phys.* **85** 1026–36
- [38] Kinane C J, Loving M, De Vries M A, Fan R, Charlton T R, Claydon J S, Arena D A et al 2014 Observation of a temperature dependent asymmetry in the domain structure of a Pd-doped FeRh epilayer *New J. Phys.* **16** 113073
- [39] Lu W, Nam N T and Suzuki T 2009 Effect of Pt doping on the structure, magnetic, and magneto-optical properties of ordered FeRh–Pt thin films *IEEE Trans. Magn.* **45** 2716–9
- [40] Pallavi Kushwaha A L, Rawat R and Chaddah P 2010 Influence of thermal annealing and magnetic field on first order magnetic transition in Pd substituted FeRh *J. Phys.: Conf. Ser.* **200** 032038
- [41] Kamenev K, Arnola Z, Kamaráda J and Baranov N V 1997 Pressure induced antiferromagnetism in  $(\text{Fe}_{1-x}\text{Ni}_x)_{49}\text{Rh}_{51}$  alloys *J. Alloys Compd.* **252** 5680–2
- [42] Barua R, Jiménez-Villacorta F and Lewis L H 2013 Predicting magnetostructural trends in FeRh-based ternary systems *Appl. Phys. Lett.* **103** 102407
- [43] Maat S, Thiele J U and Fullerton E E 2005 Temperature and field hysteresis of the antiferromagnetic-to-ferromagnetic phase transition in epitaxial FeRh films *Phys. Rev. B* **72** 214432
- [44] Ohtani Y and Hatakeyama I 1994 Features of broad magnetic transition in FeRh thin-film *J. Magn. Magn. Mater.* **131** 339–44
- [45] Heeger A J 1970 Pressure dependence of the FeRh first-order phase transition *J. Appl. Phys.* **41** 4751–2
- [46] Vinokurova L I, Vlasov A V and Pardavi-Horvath M 1976 Pressure effects on magnetic phase transitions in FeRh and FeRhIr alloys *Phys. Status Solidi b* **78** 353–7
- [47] Suzuki I et al 2009 Stability of ferromagnetic state of epitaxially grown ordered FeRh thin films *J. Appl. Phys.* **105** 1–3
- [48] Suzuki I et al 2011 Clear correspondence between magnetoresistance and magnetization of epitaxially grown ordered FeRh thin films *J. Appl. Phys.* **109** 3
- [49] Baldasseroni C et al 2014 Effect of capping material on interfacial ferromagnetism in FeRh thin films *J. Appl. Phys.* **115** 043919
- [50] Bordel C, Juraszek J, Cooke D W, Baldasseroni C, Mankovsky S, Minár J, Ebert H, Moyerman S, Fullerton E E and Hellman F 2012 Fe spin reorientation across the metamagnetic transition in strained FeRh thin films *Phys. Rev. Lett.* **109** 117201
- [51] Lu W, Yan B and Suzuki T 2009 Magnetic phase transition and magneto-optical properties in epitaxial  $\text{FeRh}_{0.95}\text{Pt}_{0.05}$ (001) single-crystal thin film *Scr. Mater.* **61** 851–4
- [52] Kinane C J et al 2014 Observation of a temperature dependent asymmetry in the domain structure of a Pd-doped FeRh epilayer *New J. Phys.* **16** 113073
- [53] Uhlíř V, Arregi J A and Fullerton E E 2016 Colossal magnetic phase transition asymmetry in mesoscale FeRh stripes *Nat. Commun.* **7**
- [54] Baldasseroni C et al 2015 Temperature-driven growth of antiferromagnetic domains in thin-film FeRh *J. Phys.: Condens. Matter* **27** 256001
- [55] Ding Y et al 2008 Bulk and near-surface magnetic properties of FeRh thin films *J. Appl. Phys.* **103** 07B515

- [56] Fan R *et al* 2010 Ferromagnetism at the interfaces of antiferromagnetic FeRh epilayers *Phys. Rev. B* **82** 184418
- [57] Smekhova A, Ciuculescu D, Lecante P, Wilhelm F, Amiens C, Rogalev A and Chaudret B 2008 X-ray magnetic circular dichroism studies of FeRh nanoparticles *IEEE Trans. Magn.* **44** 2776
- [58] Stamm C, Thiele J-U, Kachel T, Radu I, Ramm P, Kosuth M, Minár J, Ebert H, Dürr H and Eberhardt W 2008 Antiferromagnetic–ferromagnetic phase transition in FeRh probed by x-ray magnetic circular dichroism *Phys. Rev. B* **77** 184401
- [59] Bennett S P *et al* 2015 Direct evidence of anomalous interfacial magnetization in metamagnetic Pd doped FeRh thin films *Sci. Rep.* **5** 9142
- [60] [periodictable.com/Properties/A/LatticeConstants.html](http://periodictable.com/Properties/A/LatticeConstants.html)
- [61] Zakharov A I *et al* 1964 Magnetic and magnetoelastic properties of a metamagnetic Fe–Rh alloy *J. Exp. Theor. Phys.* **46** 1348–53
- [62] Ricodeau J A and Melville D 1972 Model of the antiferromagnetic–ferromagnetic transition in FeRh alloys *J. Phys. F: Met. Phys.* **2** 337
- [63] Zabel H 1999 Magnetism of chromium at surfaces, at interfaces and in thin films *J. Phys.: Condens. Matter* **11** 9303
- [64] Fullerton P R L *et al* 1995 Suppression of biquadratic coupling in Fe/Cr(001) superlattices below the Neel transition of Cr vol 75
- [65] People R and Bean J C 1985 Calculation of critical layer thickness versus lattice mismatch for  $\text{Ge}_x\text{Si}_{1-x}/\text{Si}$  strained-layer heterostructures *Appl. Phys. Lett.* **47** 322–4
- [66] Bjorck M and Andersson G 2007 GenX: an extensible x-ray reflectivity refinement program utilizing differential evolution *J. Appl. Crystallogr.* **40** 1174–8
- [67] Cao J, Nam N T, Inoue S, Ko H Y Y, Phuoc N N and Suzuki T 2008 Magnetization behaviors for FeRh single crystal thin films *J. Appl. Phys.* **103** 07F501
- [68] De Vries M A, Loving M, McLaren M, Brydson R M D, Liu X, Langridge S, Lewis L H and Marrows C H 2014 Asymmetric ‘melting’ and ‘freezing’ kinetics of the magnetostructural phase transition in B2-ordered FeRh epilayers *Appl. Phys. Lett.* **104** 232407
- [69] Nikitin S A, Myalikgulyev G, Annaorazov M P, Tyurin A L, Myndyev R W and Akopyan S A 1992 Giant elastocaloric effect in FeRh alloy *Phys. Lett. A* **171** 234–6
- [70] Suzuki I, Koike T, Itoh M, Taniyama T and Sato T 2009 Stability of ferromagnetic state of epitaxially grown ordered FeRh thin films *J. Appl. Phys.* **105** 07E501
- [71] Koenig C 1982 Self-consistent band structure of paramagnetic, ferromagnetic and antiferromagnetic ordered FeRh *J. Phys. F: Met. Phys.* **12** 1123
- [72] Gschneidner K A Jr, Pecharsky V K and Tsokol A O 2005 Recent developments in magnetocaloric materials *Rep. Prog. Phys.* **68** 1479
- [73] Nordblad P 2013 Magnetocaloric materials: strained relations *Nat. Mater.* **12** 11–2
- [74] Caron L, Trung N T and Brück E 2011 Pressure-tuned magnetocaloric effect in  $\text{Mn}_{0.93}\text{Cr}_{0.07}\text{CoGe}$  *Phys. Rev. B* **84** 020414
- [75] Lewis L H, Yu M H and Gambino R J 2003 Simple enhancement of the magnetocaloric effect in giant magnetocaloric materials *Appl. Phys. Lett.* **83** 515–7
- [76] Stern-Taulats E, Castán T, Planes A, Lewis L H, Barua R, Pramanick S, Majumdar S and Mañosa L 2017 Giant multicaloric response of bulk  $\text{Fe}_{49}\text{Rh}_{51}$  *Phys. Rev. B* **95** 104424
- [77] Barua R, McDonald I, Jiménez-Villacorta F, Heiman D and Lewis L H 2016 Multivariable tuning of the magnetostructural response of a Ni-modified FeRh compound *J. Alloys Compd.* **689** 1044–50
- [78] Chirkova A, Bittner F, Nenkov K, Baranov N V, Schultz L, Nielsch K and Woodcock T G 2017 The effect of the microstructure on the antiferromagnetic to ferromagnetic transition in FeRh alloys *Acta Mater.* **131** 31–8
- [79] Mander J B, Priestley M J N and Park R 1988 Theoretical stress–strain model for confined concrete *J. Struct. Eng.* **114** 1804–26